Harmonic-Based Phase-Shifted Control of Inductively Coupled Power Transfer

Hua Cai, Liming Shi, *Member, IEEE*, and Yaohua Li

***Abstract*—It is a key issue for inductively coupled power transfer system that the output power is regulated with high efficiency especially over a wide load range. In this paper, a novel harmonic-based phase-shifted control method is proposed. With this method, the harmonic component other than the fundamental component of the resonant inverter output voltage is employed to regulate the transferred power. The output power is controlled by changing the phase-shifted angle of the inverter. Different from the conventional approaches, the switching frequency in this method is much lower than the resonant frequency, meaning much reduced switching losses. The operation principle, switching strategy, and dead-time effect have all been presented. Experimental results demonstrate that the proposed power control method can achieve significant performance improvement at the light-load condition.**

***Index Terms*—Efficiency, harmonic, inductively coupled power transfer (ICPT), phase-shifted control, power regulation.**

NOMENCLATURE

$L_{\rm p}$	Total inductance of the primary winding.
$L_{\rm s}$	Total inductance of the secondary winding.
M	Mutual inductance.
$C_{\rm p}$	Resonant capacitor on the primary side.
$C_{\rm s}$	Resonant capacitor on the secondary side.
$R_{\rm p}$	Total resistance of the primary winding.
$R_{\rm s}$	Total resistance of the secondary winding.
$R_{\rm L}$	Load resistance.
$R_{\rm e}$	Equivalent resistance of load.
$Z_{{\rm p}k}$	Self-impedance of the kth-order harmonic component on the primary side.
$Z_{{\rm s}k}$	Self-impedance of the kth-order harmonic component on the secondary side.
$Z_{\rm r}$	Reflected impedance of the secondary circuit as seen by the primary side.
$S_1 - S_4$	Switching components.
$D_1 - D_4$	Freewheeling diodes.
$D_5 - D_8$	Diodes.
$C_{\rm f}$	Filter capacitor.
$U_{\rm dc}$	Voltage of dc input source.
$U_{\rm inv}$	Inverter output voltage.
$U_{{\rm p}k}$	Root mean square value of the kth-order harmonic component of $U_{\rm inv}$.
$U_{{\rm Re}k}$	Voltage of equivalent resistance of the kth-order harmonic component.
$U_{\rm RL}$	Voltage of load resistance.
$I_{\rm p}$	Inverter output current.
$I_{{\rm p}k}$	Inverter output current of the kth-order harmonic component.
$I_{{\rm s}k}$	Secondary winding current of the kth-order harmonic component.
$f_{\rm s}$	Switching frequency.
$f_{\rm r}$	Resonant frequency.
$\omega_{\rm s}$	Switching angular frequency.
$\omega_{\rm r}$	Resonant angular frequency.
α	Phase-shifted angle.
$t_{\rm d}$	Dead time of inverter.
$P_{\rm out}$	Output power on load.
η	Transfer efficiency.

Manuscript received November 27, 2012; revised February 22, 2013; accepted March 25, 2013. Date of current version August 20, 2013. This work was supported in part by the "Key Projects in the National Science and Technology Pillar Program during the Eleventh Five-Year Plan Period" under Grant 2007BAG02A04. Recommended for publication by Associate Editor B. Wang.

The authors are with the Key Laboratory of Power Electronics and Electric Drive, Institute of Electrical Engineering, Chinese Academy of Sciences, Beijing 100190, China (e-mail: 999hua@163.com, limings@mail.iee.ac.cn, yhli@mail.iee.ac.cn).

Digital Object Identifier 10.1109/TPEL.2013.2257865

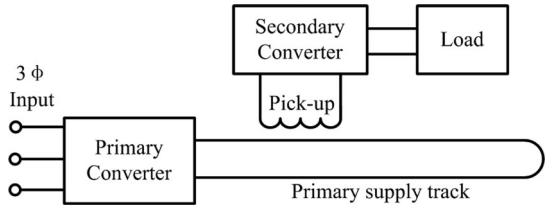

Fig. 1. Typical movable ICPT system.

I. INTRODUCTION

INDUCTIVELY coupled power transfer (ICPT) system utilizes varying magnetic field at a certain frequency to couple power across an air gap to one or more secondary load systems without direct physical contact [1], [2]. ICPT system is safe, reliable, flexible, and environment friendly due to the electrical isolation of the system. It has many applications including portable electronic devices [3], electric vehicles [4], [5], underwater power supply [6], automotive guided vehicles [7], and mining applications [8].

Rail transit system is one of the potential important applications of the ICPT system. Generally, the third rail or overhead line and pantograph are utilized to supply power for the vehicle [9]. Insufferable defects of this supply method are friction, sparks, risk of electric shock, and high maintenance cost. The movable contactless power transfer (MCPT) system is an alternative proposal for the supply of rail transit system (see Fig. 1). The MCPT system contains the ground part and vehicle part; the primary windings are powered by converter located on the

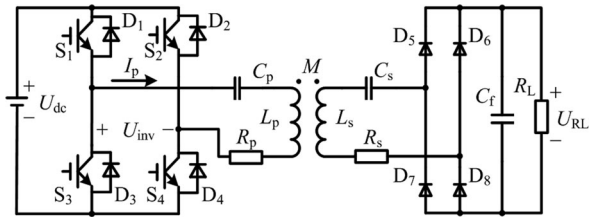

Fig. 2. Circuit topology of ICPT with series compensation.

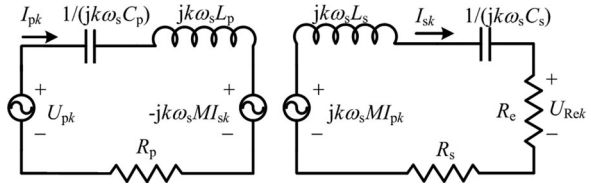

Fig. 3. Harmonic model equivalent circuit of ICPT with series compensation.

ground and the secondary windings pick up the power and then transfer it to vehicle load. Researchers presented a roadway-powered vehicle with contactless power supply system in [10] and [11]. An inductive power supply system for maglev was introduced in [12]. A tram in a city with contactless power supply system attached importance in Germany [13].

For high-power application, it is necessary to regulate the output power of ICPT system with the load change. The early output power regulation method was to change the input dc voltage of inverter by the buck or boost converter. This method is simple, but it increases the power losses, size, and cost of the primary converter. A new series ac-processing pickup was utilized to eliminate the need of an extra buck converter for controlling the output load voltage [14], which was controlled on the secondary sides. A method of varying the phase-shifted angle of the full-bridge inverter was presented to regulate the fundamental of output voltage [15]. Li *et al*. proposed an energy discontinuous injection and the free oscillation method. With this method, the switching frequency is low with high frequency of output current, but the current waveforms have a small fluctuation [16]. Four steady-state zero current switching (ZCS) operating points were adopted in [17], but the output voltage is not smooth. Choi *et al*. compared the four power conversion methods (voltage control, duty-cycle control, frequency control, and phase-shifted control) for the wireless charging system [18], and the phase-shifted control is considered to be the optimal scheme under the uniform load condition.

The objective of this paper is to improve the performance of the ICPT system at wide load range, especially at light load. First, the fundamental principle of ICPT is analyzed. Then, a harmonic model equivalent circuit for ICPT with series capacitor on both sides is built. After that, the harmonic-based phase-shifted control (HPSC) method is derived. Comparative analyses and experiments for the proposed and the conventional methods are investigated.

II. Fundamental Principle

A typical circuit topology of an ICPT system for rail transit application is shown in Fig. 2. It contains a set of primary winding coils near and along the rail, one or more secondary windings coil beneath the vehicle on board, primary converter, and secondary converters [19]. The primary converter transfers the three-phase 50 Hz ac source into dc voltage, then the inverter outputs high-frequency ac current to the primary winding coil and sets up high-frequency magnetic field. The high-frequency voltage is induced in the secondary winding coils which couple with the magnetic field. The secondary converter transforms the ac voltage to dc voltage for the load $R_{\rm L}$, which represents inverter and motor.

To increase the transferred power, compensation capacitors are used in the secondary circuit usually. On the other hand, to decrease the apparent power of the primary converter, compensation capacitors are also used in the primary circuits. Typical topologies are series capacitor compensation, parallel capacitor compensation, and more complex resonant circuit [20]. It is known that if both primary and secondary compensation capacitors are connected serially, the capacitance needed does not vary with load or with the mutual inductance between primary winding and secondary winding. So this paper adopts this compensation topology.

As discussed in Section I, the phase-shifted control for the full-bridge inverter is suitable to adjust the output power. In Fig. 2, the drive pulse duty width of each switching device is 50%, pulses of switch S_4 and S_2 lag that of S_1 and S_3 a certain phase angle α, the range of α is from 0° to 180°.

In the conventional method, the power is transferred by fundamental component, and harmonic components are usually neglected. So, the conventional phase-shifted control is called fundamental-based phase-shifted control (FPSC) in this paper. To analyze the harmonic components, fast Fourier transform (FFT) of the inverter output voltage is carried out at first. Here, the dead time of inverter is not considered, the root-mean-square (RMS) value of the kth-order harmonic component of inverter output voltage is given by

$$U_{{\rm p}k} = \frac{2\sqrt{2}}{k\pi} U_{\rm dc} \cos\frac{k\alpha}{2} (k = 1, 3, 5, 7 \ldots). \tag{1}$$

The fundamental model equivalent circuit of ICPT system is presented in [21]. Similarly, the kth-order harmonic model is built in this paper to analyze the effect of the harmonic components as well as the fundamental to the transferred power. The harmonic model equivalent circuit with series capacitors on both sides is shown in Fig. 3.

As indicated in Fig. 3, the primary current $I_{{\rm p}k}$ and secondary current $I_{{\rm s}k}$ can be expressed as

$$\begin{bmatrix} I_{{\rm p}k} \\ I_{{\rm s}k} \end{bmatrix} = \frac{U_{{\rm p}k}}{Z_{{\rm p}k} Z_{{\rm s}k} + (k\omega_{\rm s} M)^2} \begin{bmatrix} Z_{{\rm s}k} \\ {\rm j}k\omega_{\rm s} M \end{bmatrix} \tag{2}$$

where

$$\omega_{\rm s} = 2\pi f_{\rm s} \tag{3}$$

$$R_{\rm e} = \frac{8}{\pi^2} R_{\rm L} \tag{4}$$

TABLE I
SIMULATION AND EXPERIMENTAL PARAMETERS

Symbol	Value	Symbol	Value
U_{dc} (V)	90	R_p (Ω)	0.1
L_p (uH)	39	R_s (Ω)	0.2
L_s (uH)	149	C_p (uF)	0.36
M (uH)	16	C_s (uF)	0.09
R_L (Ω)	20	f_r (kHz)	42

$$Z_{pk} = \mathrm{j}k\omega_s L_p + \frac{1}{\mathrm{j}k\omega_s C_p} + R_p \tag{5}$$

$$Z_{sk} = \mathrm{j}k\omega_s L_s + \frac{1}{\mathrm{j}k\omega_s C_s} + R_s + R_e. \tag{6}$$

The kth-order harmonic component P_{ok} in output power is expressed as

$$P_{ok} = I_{sk}^2 R_e = \frac{8\cos^2\left(\frac{k\alpha}{2}\right)}{k^2\pi^2} \frac{U_{dc}^2 (k\omega_s M)^2 R_e}{\left|Z_{pk} Z_{sk} + (k\omega_s M)^2\right|^2}. \tag{7}$$

In order to analyze the variables in output power conveniently, some assumptions are made as follows. U_{dc} is considered as a constant within a switching period because the U_{dc} changes very slowly compared with the switching frequency. The parameters of the contactless transformer are constant if the skin effect and the proximity effect are ignored.

It is convinced of that both the primary and the secondary converters operate at resonance if (8) and (9) are satisfied. The impedances Z_{pk} and Z_{sk} become purely resistive, and the maximum power transfer capability is achieved [20]. The P_{ok} is then the function of the following two independent variables: ω_s and α. The former is determined by the switching frequency and the latter is the pulse phase-shifted angle of inverter

$$\omega_r = \frac{1}{\sqrt{L_p C_p}} = \frac{1}{\sqrt{L_s C_s}} \tag{8}$$

$$\omega_s = \frac{\omega_r}{k}. \tag{9}$$

In the conventional FPSC, the switching frequency is equal to the resonant frequency, and the output power is regulated by changing α. However, the switching losses increase as α approaching to 180°, which results in poor efficiency at the light-load condition. If harmonic components are utilized, the switching losses may decrease due to the low switching frequency. From analyses aforementioned, the condition to transfer power by harmonic is (9). In other words, the harmonic frequency selected should equal to resonant frequency by decreasing the switching frequency.

To vividly describe the contribution of the harmonic components to transferred power, output power is plotted according to (7) in Fig. 4. In this figure, (a), (b), and (c) correspond to the switching frequencies 42, 14, and 8.4 kHz, respectively, under the condition of pulse phase-shifted angle α being zero. Other parameters are shown in Table I. It indicates in the Fig. 4 that if the switching frequency is selected as (9) the output power is mainly transferred by the harmonic component at the resonant frequency. What is more, the transferred power by the third-order harmonic and fifth-order harmonic component is nearly 1/9 and 1/25 times that of the fundamental component.

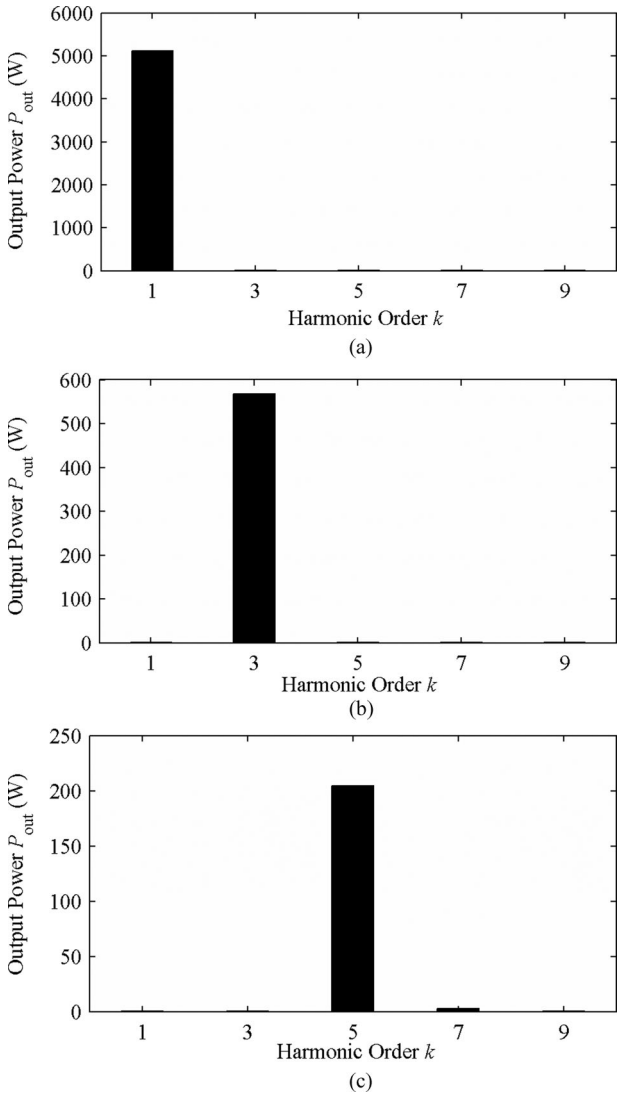

Fig. 4. Output power with different harmonic components under $f_r = 42$ kHz: (a) $f_s = 42$ kHz, (b) $f_s = 14$ kHz, and (c) $f_s = 8.4$ kHz.

III. THE HARMONIC-BASED PHASE-SHIFTED CONTROL

A. The Harmonic-Based Phase-Shifted Control

As analyzed in the previous section , the harmonic components of inverter output voltage can be used to transfer power by changing switching frequency. Besides, to regulate output power accurately, phase-shifted control is used. Detailed analysis of HPSC is as follow.

At first, harmonic components of inverter output voltage must be found out. To show it generally, normalized value is introduced. Based on the RMS value of fundamental component of the inverter output voltage U_{p1} at zero phase-shifted angle, the normalized value of the kth-order harmonic RMS value at

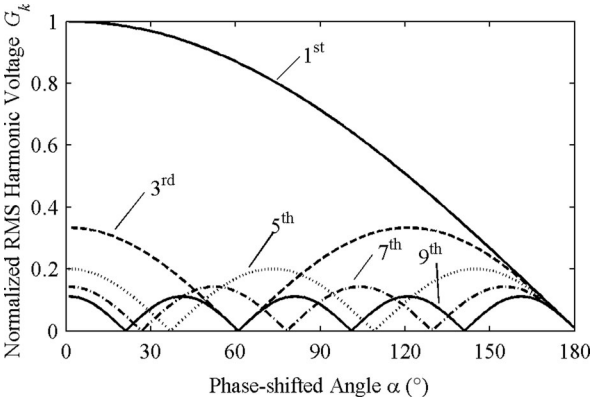

Fig. 5. Normalized value of fundamental and harmonic components at different phase-shifted angle.

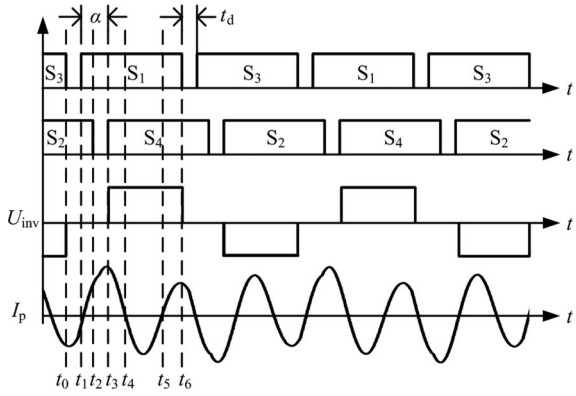

Fig. 6. Key waveforms of HPSC with third-order harmonic.

phase-shifted angle α is expressed as

$$G_k = \frac{U_{pk}}{U_{p1}} = \frac{1}{k}\cos\frac{k\alpha}{2}(k = 1, 3, 5, 7\ldots). \tag{10}$$

Fig. 5 shows the normalized value of fundamental and harmonic components at different phase-shifted angle α, where 1st means the fundamental component, 3rd, 5th, 7th, and 9th mean the high-order harmonic component, respectively. Here, more harmonics are not revealed due to the limited pages.

In Fig. 5, fundamental component gets smaller with phase-shifted angle approaching to 180°. The maximum value of normalized value of the kth-order harmonic G_k is 1/k according to (10). Once G_1 becomes less than 1/k, the kth-order harmonic component instead of fundamental component can be used to transfer the same capacity of power. The switching frequency could be decreased to 1/k times of the resonant frequency. The output power can be regulated by the changing phase-shifted angle.

To illustrate this method, Fig. 6 shows key waveforms of the third-order harmonic-based phase-shifted control method. Furthermore, a half switching period in Fig. 6 is subdivided into six stages and their simplified paths in different stages are shown in Fig. 7.

Stage 1 [t_0, t_1]: S_3 turns OFF at t_0. From t_0 to t_1, the power is oscillating freely through S_2, L_p, Z_r, R_p, C_p, and D_1. U_{inv} is equal to 0 during this stage.

Stage 2 [t_1, t_2]: At t_1, S_1 turns ON at zero voltage switching (ZVS) when D_1 conducts. The power is oscillating freely through S_1, C_p, R_p, Z_r, L_p, and D_2.

Stage 3 [t_2, t_3]: At t_2, S_2 turns OFF at ZVS when D_2 conducts.

Stage 4 [t_3, t_4]: S_4 turns ON at t_3, and D_2 turns OFF at the same time. The conduction current through S_4 is same with the turning OFF current of D_2. The power is transferred from input dc source to load through S_1, C_p, R_p, Z_r, L_p, and S_4. U_{inv} is equal to U_{dc} during this stage.

Stage 5 [t_4, t_5]: Inverter output current I_p crosses zero and changes its direction at t_4. The power is circulated from load to input dc source through D_4, L_p, Z_r, R_p, C_p, and D_1. This stage finishes when I_p reaches zero.

Stage 6 [t_5, t_6]: After the current I_p crosses zero and changes its direction at t_5, the power is transferred from input dc source to load through S_1, C_p, R_p, Z_r, L_p, and S_4 during this stage. This stage ends when S_1 turns OFF at t_6.

The stages of the other half period are similar with that of above. The current I_p circulates three times during one switching period, which means lower switching losses compared with FPSC.

For higher order harmonic-based phase-shifted control, there will be more current circulation during one switching period and lower switching losses.

B. Switching Strategy for Harmonic Components

From Fig. 5, it is evident that several harmonic components meet the demand of low output power. The switching strategy for different order harmonic is discussed as follows.

First, α_{1k} is defined as the switching phase-shifted angle from fundamental to the kth-order harmonic component. When fundamental component is at resonance, the kth-order harmonic component could be employed to transfer the same power if the phase-shifted angle is greater than α_{1k}. The maximum value of G_k is 1/k, so from the relationship $G_1 = 1/k$, α_{1k} can be expressed as

$$\alpha_{1k} = \frac{360^\circ}{\pi}\arccos\frac{1}{k}(k = 1, 3, 5, 7\ldots). \tag{11}$$

Similarly, α_k is defined as switching phase-shifted angle from the kth-order harmonic to $(k + 2)$ th-order harmonic. When the k-th-order harmonic is at resonance, if the phase-shifted angle is greater than α_k, then $(k + 2)$ th-order harmonic can be used to transfer same capacity of power. It means the reasonable phase-shifted angle range of the kth-order harmonic can be 0 to α_k. From the relationship $G_k = 1/(k+2)$, α_k can be expressed as

$$\alpha_k = \frac{360^\circ}{k\pi}\arccos\frac{k}{k+2}(k = 1, 3, 5, 7\ldots). \tag{12}$$

The switching phase-shifted angles for fundamental and harmonic components are shown in Table II.

According to (7) and (10), ignore the components which are not at resonance, the normalized value of output power is

$$G_{p_k} = G_k^2 = \frac{1}{k^2}\cos^2\frac{k\alpha}{2}(k = 1, 3, 5, 7\ldots). \tag{13}$$

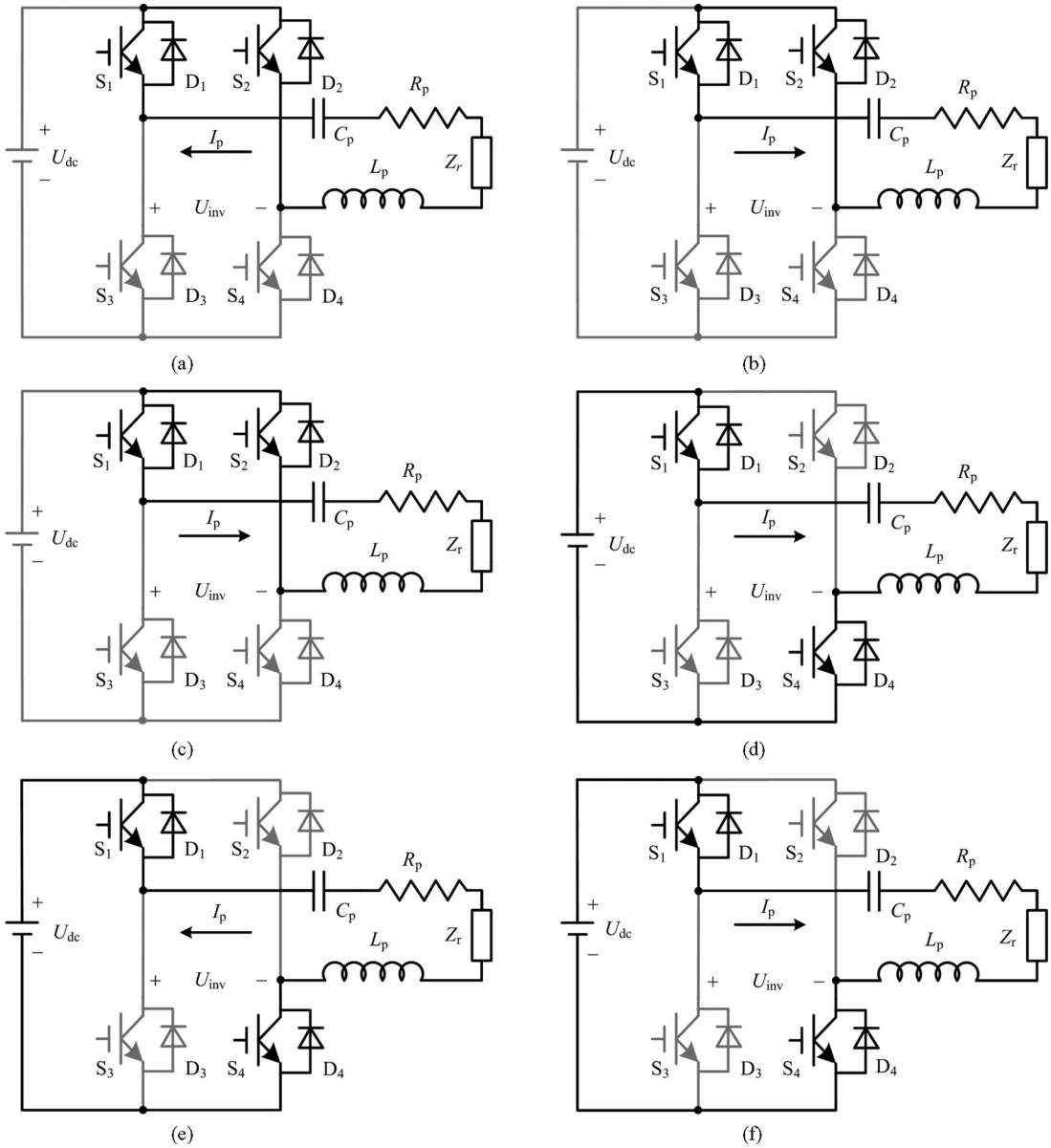

Fig. 7. Simplified paths of HPSC with third-order harmonic in half switching period.

TABLE II
SWITCHING PHASE-SHIFTED ANGLES FOR FUNDAMENTAL AND HARMONICS

Harmonic order	α_{1k} (°)	α_k (°)
1	0	141.1
3	141.1	35.4
5	156.9	17.8
7	163.6	11.1
9	167.2	7.8
k	$\frac{360^\circ}{\pi}\arccos\frac{1}{k}$	$\frac{360^\circ}{k\pi}\arccos\frac{k}{k+2}$

TABLE III
NORMALIZED OUTPUT POWER AND PHASE-SHIFTED ANGLE RANGE

Harmonic order	G_{pk}	Phase-shifted angle range for FPSC (°)	Phase-shifted angle range for HPSC (°)
1	11.1%~100%	141.1	141.1
3	4.0%~11.1%	15.8	35.4
5	2.0%~4.0%	6.7	17.8
7	1.2%~2.0%	3.6	11.1
k	$\frac{1}{(k+2)^2}\sim\frac{1}{k^2}$	$\alpha_{1(k+2)}$-α_{1k}	α_k

So, the reasonable normalized output power range of the kth-order harmonic is from $1/(k+2)^2$ to $1/k^2$. Table III shows the reasonable normalized output power range in percentage and phase-shifted angle range for fundamental and harmonic components. The normalized output power range of HPSC is less than $1/3^2$ or 11.1% theoretically, and the phase-shifted range for

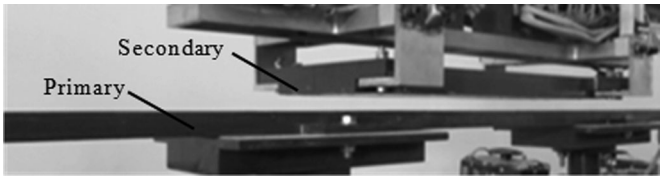

Fig. 8. Photo of the movable contactless transformer.

harmonic component is much wider than that for fundamental. In fact, the range of normalized output power is a little higher since the maximum output power decreased due to the dead time of an inverter.

C. Effect of the Dead Time

The dead time is necessary to avoid current passing directly through any bridge arm of an inverter. Because it will bring some effect to duty width, it must be considered especially for high frequency switching. For example, the effective duty width will be decreased from 50% to 41.6% if dead time is 2 μs and switching frequency is 42 kHz, which results in decreased maximum output power. Here, α_{kd} is defined as equivalent phase-shifted angle of dead time for the kth order harmonic in HPSC, and it is expressed as

$$\alpha_{\mathrm{kd}} = \frac{t_{\mathrm{d}} f_{\mathrm{r}} 360^{\circ}}{k} (k = 1, 3, 5, 7 \ldots). \tag{14}$$

Considering the dead time effect, the equations with phase-shifted angle α will be updated. Taking $U_{\mathrm{p}k}$ as an example, (1) is updated as

$$U'_{\mathrm{p}_k} = \frac{2\sqrt{2}}{k\pi} U_{\mathrm{dc}} \cos \frac{k(\alpha + \alpha_{kd})}{2} (k = 1, 3, 5, 7 \ldots). \tag{15}$$

Besides, the switching phase-shifted angle will be updated as

$$\alpha'_{1\mathrm{k}} = \frac{360^{\circ}}{\pi} \arccos \frac{1}{k} - t_{\mathrm{d}} f_{\mathrm{r}} 360^{\circ} (k = 1, 3, 5, 7 \ldots) \tag{16}$$

$$\alpha'_{k} = \frac{360^{\circ}}{k\pi} \arccos \frac{k}{k+2} - \frac{t_{\mathrm{d}} f_{\mathrm{r}} 360^{\circ}}{k} (k = 1, 3, 5, 7 \ldots). \tag{17}$$

It is evident that the phase-shifted angle for the maximum value of $U'_{\mathrm{p}k}$ (k = 3,5,7...) is $\frac{360^{\circ}}{k} - \alpha_{kd}$ instead of zero. The lost phase-shifted angle range due to the dead time can be replaced by $\frac{360^{\circ}}{k} - \alpha_{kd} \sim \frac{360^{\circ}}{k}$.

IV. Experimental Results

A. Experimental Setup

In order to verify the validity of HPSC power regulation method, experiments have been implemented on a prototype of movable contactless power supply system for rail transit. The prototype consists of a contactless transformer and two converters.

The contactless transformer contains long primary winding and short secondary winding. The former is fixed on ground along the track, and the latter is fixed on the movable vehicle. The photo is shown in Fig. 8. Its dimensions are listed in Table IV.

TABLE IV
The Contactless Transformer Dimensions

Parameters	Long (mm)	Width (mm)	Turns
Primary	1600	100	6
Secondary	560	100	12
Electromagnetic gap (mm)	25		

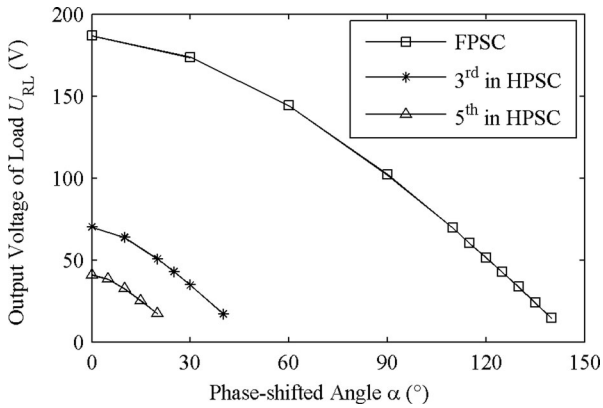

Fig. 9. Output voltage at different phase-shifted angles with different methods.

The converter topology adopted is the same as that in Fig. 2, where the dc voltage U_{dc} is obtained from a three-phase diode rectifier. The load is purely resistive. The third- and the fifth-order harmonic are chosen for experiment in this paper. The dead time is set as 2 μs. The equivalent phase-shifted angle of dead time is 30°, 10°, and 6° for FPSC, third-order harmonic in HPSC, and fifth-order harmonic in HPSC respectively.

B. Power Regulation Comparison

Fig. 9 shows the voltage measured on load at a given phase-shifted angle for three kinds of control methods. It is known that the curves in Fig. 9 are very similar with those in Fig. 5, because the U_{RL} is nearly proportional to $U_{\mathrm{p}k}$. It can be seen that the higher the harmonic order is, the lower the maximum output power is. It is apparently consistent with aforementioned analyses.

The phase-shifted angle range under the same range of output power for FPSC, the third-order harmonic and fifth-order harmonic in HPSC is compared. According to the analysis in Section III, output power is lower with higher harmonic order, so the reasonable range $1/7^2 \sim 1/5^2$ of normalized output power of the fifth-order harmonic in HPSC is selected. According to (13), the start phase-shifted angle for the selected normalized power range can be obtained from (18) and the end phase-shifted angle is obtained from (19). Then the phase-shifted angle range can be calculated

$$G_{\mathrm{p}_k} = 1/5^2 \ (k = 1, 3, 5) \tag{18}$$

$$G_{\mathrm{p}_k} = 1/7^2 \ (k = 1, 3, 5). \tag{19}$$

A comparison of phase-shifted angle range during the same range of normalized output power is shown in Table V. From

TABLE V
COMPARISON OF PHASE-SHIFTED ANGLE RANGE UNDER THE SAME RANGE OF NORMALIZED OUTPUT POWER ($1/7^2 \sim 1/5^2$)

Method	Start phase-shifted angle (°)	End phase-shifted angle (°)	Phase-shifted angle range (°)
FPSC	156.9	163.6	6.7
Third-order harmonic in HPSC	35.4	43.1	7.7
Fifth-order harmonic in HPSC	0	17.8	17.8

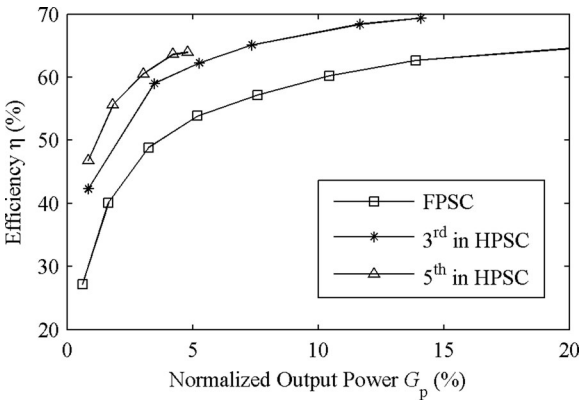

Fig. 10. System efficiency with different methods at light load.

this table, it can be known that phase-shifted angle range is wider if higher order harmonic is used. The wider phase-shifted angle range means higher power regulation accuracy due to the limited digital bits in digital processor.

C. Efficiency Comparison

In order to verify the improvement of system efficiency from HPSC to usual FPSC, experiments for FPSC, the third-order harmonic in HPSC, and fifth-order harmonic in HPSC at their power range have all been tested. Here, the input power of three phase ac power and load power are measured, and then efficiency of the whole system is calculated. Similarly with G_k, the normalized value $G_{\rm p}$ of output power is expressed as (20). The base value $P_{o\max}$ is the max value of output power at actual zero phase-shifted angle using FPSC. The $P_{o\max}$ here is 1.744 kW.

$$G_{\rm p} = \frac{P_{\rm out}}{P_{\rm o\max}}. \tag{20}$$

Fig. 10 shows the efficiency at light load with these three methods. It can be seen that 1) system efficiency increased with higher output power; 2) system efficiency using HPSC is higher than that of FPSC at the same output power; 3) efficiency of the fifth-order harmonic in FPSC is higher than that of the third-order harmonic in HPSC; and 4) the suitable $G_{\rm p}$ for HPSC is about less than 15% in fact.

D. Comparison under the Same Output Power

To compare the proposed HPSC and the conventional FPSC under the same output power, the following experiment is implemented. The output power here is about 88 W and $G_{\rm p}$ is around 5%. Detailed experiment data are shown in Table VI. As can be seen from this table, the fifth-order harmonic in HPSC improves efficiency of system with 10.09% compared to FPSC. It can be inferred that higher efficiency improvement will be reached at lighter load.

TABLE VI
EXPERIMENTAL DATA WITH DIFFERENT CONTROL METHODS

Method	f_s (kHz)	α (°)	$U_{\rm RL}$ (V)	η (%)
FPSC	42.0	125	42.6	53.85
Third order harmonic in HPSC	14.0	25	42.9	62.27
Fifth order harmonic in HPSC	8.4	0	41.0	63.94

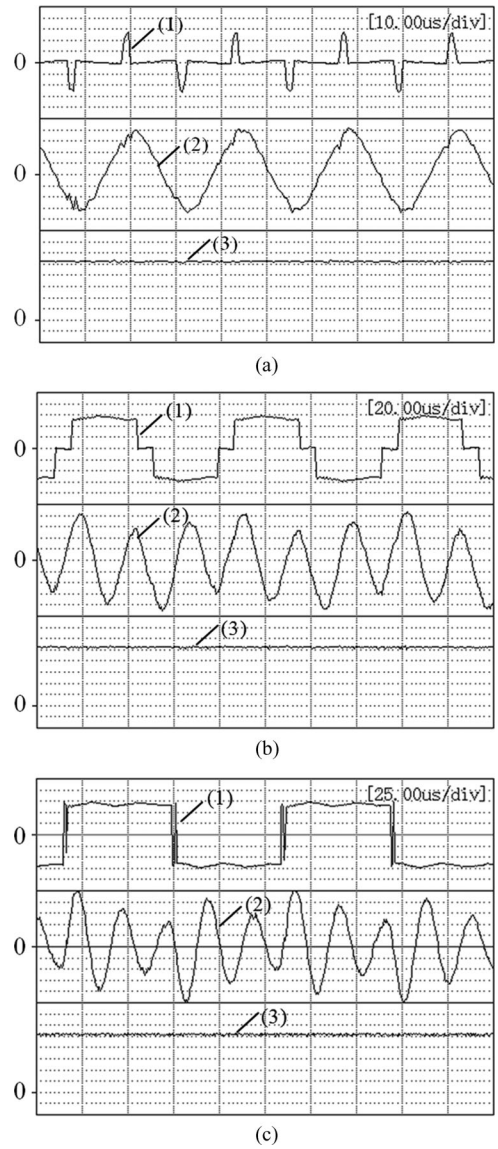

Fig. 11. Waveforms of the inverter output voltage and current using different control methods. (a) FPSC. (b) Third-order harmonic in HPSC. (c) Fifth-order harmonic in HPSC : (1) $U_{\rm inv}$:[31.25 V/div]; (2) $I_{\rm p}$:[3.9065 A/div]; (3) $U_{\rm RL}$:[7.81 V/div].

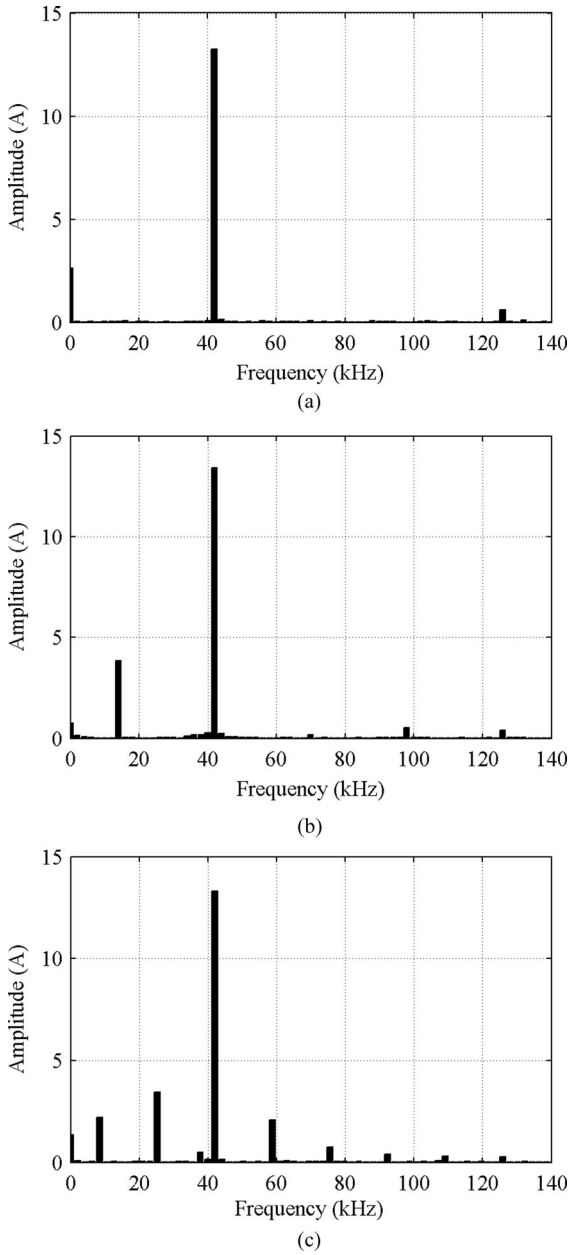

Fig. 12. FFT analysis of an inverter output current using different control methods. (a) FPSC. (b) Third-order harmonic in HPSC. (c) Fifth-order harmonic in HPSC.

Fig. 11 shows the waveforms of inverter output voltage $U_{\rm inv}$, inverter output current $I_{\rm p}$, and voltage on load $U_{\rm RL}$ with FPSC, the third-order harmonic in HPSC, and the fifth-order harmonic in HPSC, respectively.

In Fig. 11, the phase-shifted angle is great at light load for FPSC, which results in great switching losses. However, the phase-shifted angle is smaller for HPSC, and the switching frequency is much lower, which decreases switching losses remarkably.

FFT analysis to the inverter output current $I_{\rm p}$ is carried out to compare the current spectrum, which is shown in Fig. 12. As can be seen from this figure we have as follows.

1) The amplitude of inverter output current at resonant frequency is almost of the same. The reason is that the power is transferred mainly at the resonant frequency.
2) Low frequency harmonics using HPSC is greater than that of FPSC, whereas high frequency harmonics is lower. This is because the switching frequency adopted by HPSC is much lower than resonant frequency resulting that the low-order harmonic of inverter output voltage takes high proportion.
3) If higher order harmonic is employed to transfer power for HPSC, there will be more harmonic current components near the resonant frequency. Because the quality factor Q of resonant circuit is not infinite, so the harmonics components far from the resonant frequency are mostly filtered, but those near the resonant frequency do not decay seriously.

V. Conclusion

A novel power regulation method called HPSC for the full-bridge resonant converter is proposed in this paper. It utilizes harmonic component of resonant inverter output voltage other than the fundamental component to regulate the transferred power. In this method, the switching frequency is set to be much lower than the resonant frequency, but the frequency of selected harmonic component is the same with the resonant frequency. The phase-shifted angle of the inverter is controlled to regulate the output power. The efficiency increases more than 10% at the light-load condition. Analyses and experimental results shows that the proposed method can improve system efficiency remarkably compared with the traditional fundamental- based phase shift control. Furthermore, improved power regulation precision and reduced switching frequency have been achieved simultaneously. Results of the investigation demonstrate that the proposed control method for the resonant converter can effectively improve the converter performance at the light-load condition. Because of the characteristic of HPSC that harmonic component is adopted, there is a limited range of normalized output power using HPSC, which is less than 11.1% in theory.

Acknowledgment

The authors thank Dr. F. Xu, Dr. Z. Li, Y. Zhang, W. Wang for supporting in the system experiments.

References

[1] A. K. Swain, M. J. Neath, U. K. Madawala, and D. J. Thrimawithana, "A dynamic multivariable state-space model for bidirectional inductive power transfer systems," *IEEE Trans. Power Electron.*, vol. 27, no. 11, pp. 4772–4780, Nov. 2012.

[2] H. Matsumoto, Y. Neba, K. Ishizaka, and R. Itoh, "Model for a three-phase contactless power transfer system," *IEEE Trans. Power Electron.*, vol. 26, no. 9, pp. 2676–2687, Sep. 2011.

[3] Y. Ota, T. Takura, F. Sato, H. Matsuki, T. Sato, and T. Nonaka, "Impedance matching method about multiple contactless power feeding system for portable electronic devices," *IEEE Trans. Magn.*, vol. 47, no. 10, p. 4235—4237, Oct. 2011.

[4] S. Hasanzadeh, S. Vaez-Zadeh, and A.H. Isfahani, "Optimization of a contactless power transfer system for electric vehicles," *IEEE Trans. Veh. Technol.*, vol. 61, no. 8, pp. 3566–3573, Oct. 2012.

[5] G. A. J. Elliot, S. Raabe, G. A. Covic, and J. T. Boys, "Multiphase pick-ups for large lateral tolerance contactless power-transfer systems," *IEEE Trans. Ind. Electron.*, vol. 57, no. 5, pp. 1590–1598, May 2010.
[6] J. Kuipers, H. Bruning, S. Bakker, and H. Rijnaarts, "Near field resonant inductive coupling to power electronic devices dispersed in water," *Sens. Actuators A: Phys.*, vol. 178, pp. 217–222, May 2012.
[7] S. Raabe and G. A. Covic, "Practical design considerations for contactless power transfer quadrature pick-ups," *IEEE Trans. Ind. Electron.*, vol. 60, no. 1, pp. 400–409, Jan. 2013.
[8] K. W. Klontz, D. M. Divan, D. W. Novotny, and R. D. Lorenz, "Contactless power delivery system for mining applications," *IEEE Trans. Ind. Appl.*, vol. 31, no. 1, pp. 27–35, Jan./Feb. 1995.
[9] D. J. Hartland, "Electric contact systems – Passing power to the trains," in *Proc. 5th IET Prof. Develop. Course REIS*, London, U.K., 2011, pp. 60–68.
[10] J. Huh, S. W. Lee, W. Y. Lee, G. H. Cho, and C. T. Rim, "Narrow-width inductive power transfer system for online electrical vehicles," *IEEE Trans. Power Electron.*, vol. 26, no. 12, pp. 3666–3679, Dec. 2011.
[11] G. A. Covic, J. T. Boys, M. L. G. Kissin, and H. G. Lu, "A three-phase inductive power transfer system for roadway-powered vehicles," *IEEE Trans. Ind. Electron.*, vol. 54, no. 6, pp. 3370–3378, Dec. 2007.
[12] M. Bauer, P. Becker, and Q. Zheng, "Inductive power supply (IPS®) for the transrapid," presented at the Magn. Levitated Syst. Linear Drives, Dresden, Germany, 2006.
[13] (Jun. 2012). [Online]. Available: http://www.railwaygazette.com/news/urban-rail/si-ngle-view/view/primove-induction-powered-tram-trial-proves-a-success.html
[14] H. H. Wu, G. A. Covic, J. T. Boys, and D. J. Robertson, "A series-tuned inductive-power-transfer pickup with a controllable AC-voltage output," *IEEE Trans. Power Electron.*, vol. 26, no. 1, pp. 98–109, Jan. 2011.
[15] G. B. Koo, G. W. Moon, and M. J. Youn, "Analysis and design of phase shift full bridge converter with series-connected two transformers," *IEEE Trans. Power Electron.*, vol. 19, no. 2, pp. 411–419, Mar. 2004.
[16] H. L. Li, A. P. Hu, and G. A. Covic, "FPGA controlled high frequency resonant converter for contactless power transfer," in *Proc. IEEE Power Electron. Spec. Conf. 2008*, Rhodes, Greece, 2008, pp. 3642–3647.
[17] C. S. Tang, Y. Sun, Y. G. Su, S. K. Nguang, and A. P. Hu, "Determining multiple steady-state ZCS operating points of a switch-mode contactless power transfer system," *IEEE Trans. Power Electron.*, vol. 24, no. 2, pp. 416–425, Feb. 2009.
[18] W. P. Choi, W. C. Ho, X. Liu, and S. Y. R. Hui, "Comparative study on power conversion methods for wireless battery charging platform," in *Proc. EPEPower Electron. Motion Control Conf.*, Ohrid, Republic of Macedonia, 2010, pp. S15-9–S15-16.
[19] J. L. Villa, J. Sallan,A. Llombart, and J.F. Sanz, "Design of a high frequency inductively coupled power transfer system for electric vehicle battery charge," *Appl. Energy*, vol. 86, no. 3, pp. 355–363, Mar. 2009.
[20] C. S. Wang, G. A. Covic, and O. H. Stielau, "Power transfer capability and bifurcation phenomena of loosely coupled inductive power transfer systems," *IEEE Trans. Ind. Electron.*, vol. 51, no. 1, pp. 148–157, Feb. 2004.
[21] H. Cai, L. M. Shi, and R. H. Zhang, "A novel control method of resonant inverter for movable contactless power supply system of maglev," presented at the *Int. Conf. Electr. Mach. Syst.*, Beijing, China, 2011.

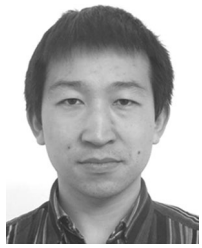

Hua Cai was born in Shanxi, China, in 1987. He received the B.Eng. degree in electrical engineering and automation from the Shandong University of Science and Technology, Qingdao, China, in 2009. He is currently working toward the Ph.D. degree in electric engineering from the Institute of Electric Engineering, Chinese Academy of Sciences, Beijing, China.

His current research interests include contactless power supply, converter, and control.

Liming Shi (M'12), was born in Henan, China, in 1964. He received the Ph.D. degree in 1998 from Kyushu University, Fukuoka, Japan.

From 1998 to 2000, he was a Postdoctoral Research Fellow in the Japan Society for the promotion of science, Japan. From 2000 to 2002, he was the Chief Researcher in Yaskawa Electric Company, Ltd., Kitakyushu, Japan. He joined the Institute of Electrical Engineering, Chinese Academy of Sciences, Beijing, China, in 2002, where he is currently a Professor. His current research interests include analysis and control of electrical machines, contactless power supply.

Yaohua Li was born in Henan, China, in 1966. He received the Ph.D. degree in 1994 from Tsinghua University, Beijing, China.

From 1995 to 1997, he was a Postdoctoral Research Fellow in the Institute of Electrical Machine, Technical University of Berlin, Berlin, Germany. He joined the Institute of Electrical Engineering, Chinese Academy of Sciences, Beijing, China, in 1997, where he is currently a Professor and Vice Director of the Institute of Electrical Engineering, Chinese Academy of Sciences. His research interests include analysis and control of electrical machines, and power electronics technology.